Application of an Inverse-Forward Approach to Derive the 12-lead ECG from Body Surface Potential Maps

Laura R Bear[1], Peter Huntjens[1,2], Mark Potse[1,3], Josselin Duchateau[1], Sylvain Ploux[1], Remi Dubois[1]

[1]IHU-LIRYC, Université de Bordeaux, Bordeaux, France
[2]CARIM School for Cardiovascular Diseases, Maastricht UMC, Maastricht, The Netherlands
[3]Inria Bordeaux Sud-Ouest. Carmen team, Bordeaux, France

Abstract

An inverse-forward approach was assessed to compute a 12-lead ECG from body surface potential mapping data. Using simulated data (n=21), reconstructed 12-lead ECGs had accurate morphology (CC>0.88), amplitude (RMSE<8.6%) and mean electrical axis during both depolarization and repolarization ($|\Delta\theta| < 17$ degrees). There was no significant deterioration in results until body surface mapping electrodes were removed within 6 cm of any 12-lead electrode ($p < 0.0001$). Reconstructed 12-lead ECGs of 6 CRT candidates captured the measured mean electrical axis during the QRS and T-wave ($|\Delta\theta| = 6.2 \pm 4.7$ and 14.2 ± 2.6 degrees respectively). Furthermore, additional clinically relevant features were reproduced allowing the correct identification of left bundle branch block and nonspecific intraventricular conduction disturbance, including: broad/notched R-waves, presence/absence of Q-wave, and direction of T-waves.

1. Introduction

High density body surface potential mapping (BSPM) provides precise detection and diagnosis of electrophysiological phenomena, either through direct analysis of BSPM [1] or through non-invasive electrocardiographic imaging of cardiac electrical activity [2]. Clinicians prefer to interpret this information in light of a 12-lead ECG, which is of daily use in cardiac arrhythmia diagnosis. However, BSPM systems are frequently missing signals in 12-lead electrode locations and alternative leads produce substantially different results [3]. This is particularly a problem during non-stable rhythms requiring concurrent measurements, as the 12-lead electrodes cannot be placed simultaneously with many commercial BSPM systems.

In this study, using simulated and clinical data, we evaluated the use of an inverse-forward approach to compute the 12-lead ECG from BSPM.

2. Methods

2.1. 12-Lead Reconstruction Algorithm

12-lead ECGs were calculated from BSPM using an inverse-forward interpolation scheme [4]. That is, signals are inversely reconstructed from BSPMs onto an arbitrary interior surface. The computed interior surface signals are used in a forward model to compute the 12-lead ECG.

Here, the inverse method was a modified version of the method of fundamental solutions (MFS) for solving the inverse problem of electrocardiography [5]. MFS coefficients of a virtual source were computed on an interior surface located near the body surface. This constitutes a Cauchy problem for Laplace's equation:

$$\nabla^2 \emptyset(x) = 0, \quad x \in \Omega \tag{1}$$

with boundary conditions:

$$(i) \quad \emptyset(x) = \emptyset_T(x) \quad x \in \Gamma_T$$
$$(ii) \quad \frac{\partial \emptyset(x)}{\partial n} = 0 \quad x \in \Gamma_T$$

where Ω is the volume between the fictitious interior surface and the torso surface Γ_T; $\emptyset(x)$ are the potentials located at x; $\emptyset_T(x)$ are the potentials on the torso surface.

Discretizing Eq (1) gives:

$$b = \mathbf{A}\, a \tag{2}$$

Where b is a vector of BSPM electrode potentials and normal derivatives, a is a vector of MFS coefficients at the intermediate interior surface, and $\mathbf{A}$ is the transfer matrix containing the geometric relationship between the two surfaces. A constant conductivity medium was assumed between the two surfaces, and Tikhonov regularization method [6] with CRESO-determined regularization parameter [7] was used to compute a. The coefficient vector a was then used as an input to compute the 9 electrodes on the torso defining the 12-lead ECG from the fictitious interior surface (Eq (2)).

The fictitious interior surface was defined by deflating the torso surface by a factor of 0.6 relative to the geometrical centre of the torso. The geometric centre was

 ISSN: 2325-887X DOI:10.22489/CinC.2017.093-231

found by computing the average coordinate value of all the torso electrodes.

2.2. Data Sets

Numerical Simulations

Simulated data were computed using a monodomain reaction-diffusion model (0.2 mm resolution) coupled to a bidomain torso model (1 mm resolution). Transmembrane ionic currents were computed with the TNNP model of the human ventricular myocyte [8]. Simulations were performed using the propag-5 software [9] on a Blue Gene/Q supercomputer. Cardiac sequences simulated included 6 paced activation, and 15 re-entrant VTs. BSPM were computed from simulated transmembrane currents using a finite-difference torso model. Heart and thoracic anatomy were created from MRI data and included intracavitary blood, anisotropic myocardium, lungs, and an anisotropic skeletal muscle layer. From the simulated torso potentials, the 12-lead ECG (gold standard) and a 252-channel BSPM recording was extracted and used here. To assess the sensitivity to missing electrodes, unusable BSPM channels were defined as all electrodes within 0, 2, 4, 6, 8, 10 and 12 cm of each of the 9 electrodes defining the 12-lead ECG respectively, for a total of 63 combinations of unusable electrodes. The 12-lead ECG electrode positions for reconstruction were the same as the gold standard.

Clinical Data

In total, 6 heart failure patients scheduled for CRT implantation (QRS width >120 ms) where included in this study: 3 patients with left bundle branch block (LBBB) and 3 with non-specific intraventricular conduction disturbance (NICD), as defined according to AHA/ACCF/HRS criteria [10]. For each patient, a 12-lead ECG (gold standard) was recorded in sinus rhythm at rest in supine position (filtered 0.5-35 Hz). BSPM were then recorded with a 252-electrode vest (CardioInsight, Medtronic) and geometric information was acquired with computed tomography (CT). Channels in which signals were absent as a result of lead fracture or poor electrode contact were defined as unusable. The 12-lead ECG placement for reconstruction were defined using the bony landmarks visible in the CT.

2.3. Comparison and Statistics

For both data sets, unusable electrodes and their associated signals were removed from the torso mesh and excluded from the formulation of the transfer matrix. Reconstructed ECG waveforms were compared to gold standards using a Pearson's correlation (CC) and root mean square error (RMSE). The absolute difference in mean electrical axis of the heart ($|\Delta\theta|$) during the QRS (pacing, sinus and VT) and T-wave (pacing and sinus) were also compared between the reconstructed and measured 12-lead ECG. The mean axis was defined using a two lead approach[11]:

$$\theta = \tan^{-1}\left(\frac{I+2III}{\sqrt{3}I}\right) \quad (5)$$

where I and III are the net voltage over the QRS or T-wave for these leads.

For each metric, normality was tested with a Shapiro-Wilk's test. The significance of differences among means was tested using an ANOVA, accounting for interaction with lead and distance of unusable electrodes. Significance was taken for $p<0.05$ Post-hoc comparisons were made using a Tukey's HSD. Data are expressed as median [LQR;UQR].

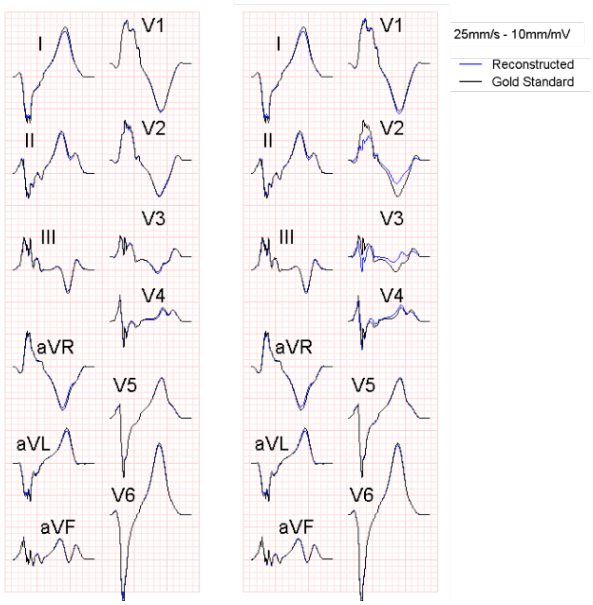

Fig 1. True and reconstructed 12-lead ECG using simulated data with no missing electrodes (left) and unusable electrodes ≤8 cm of V3 (right).

3. Results

3.1. Numerical Simulations

Raw data (CC, RMSE, and $|\Delta\theta|$) were skewed and were rendered normal with log transformations ($p<0.05$). Figures present non-transformed data.

With no unusable electrodes, reconstructed 12-lead ECGs were very accurate, with CC = 0.99 [0.99;1.00], RMSE = 0.02 [0.00;0.06] and $|\Delta\theta| = 1.6^{o}$ [0.9;3.8]. Fig. 1 (left) presents reconstructed and gold standard 12-lead ECGs for a left ventricular pacing sequence, with no obvious difference between signals.

Leads I, II and aVR had a lower CC than all other leads ($p<0.04$), while Leads I and aVR had higher RMSE ($p<0.004$). CC and RMSE values and statistics for each lead are presented in Fig 2.

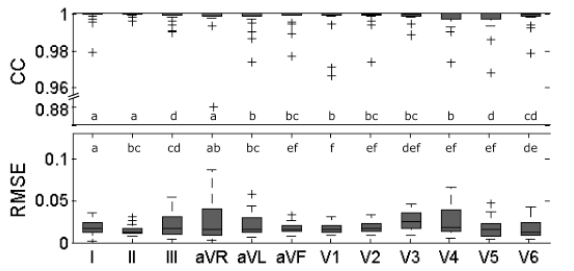

Fig 2. Reconstruction accuracy of each lead using simulated data without unusable electrodes. Crosses represent outliers. Leads with the same letter were not significantly different ($p>0.05$) from post-hoc Tukey's HSD.

With an increasing number of unusable electrodes, more outliers became evident for each metric, though the median values did not substantially change (Fig 3). Compared to no unusable electrodes (0 cm), CC and RMSE were significantly increased when unusable electrodes were ≥6 cm from the 12-lead ECG electrodes ($p<0.0001$), and $|\Delta\theta|$ when up to 12cm ($p<0.05$)

Unusable electrodes most affected reconstruction accuracy in lead they were closest to. This is demonstrated in Fig 1 (right), with V2 and V3 more altered by unusable electrodes within 8 cm of V3. Missing electrodes around left arm electrode resulted in a significantly higher $|\Delta\theta|$ than any other electrode except the right arm ($p<0.02$). This is because limb leads I and III are involved in the computation of θ.

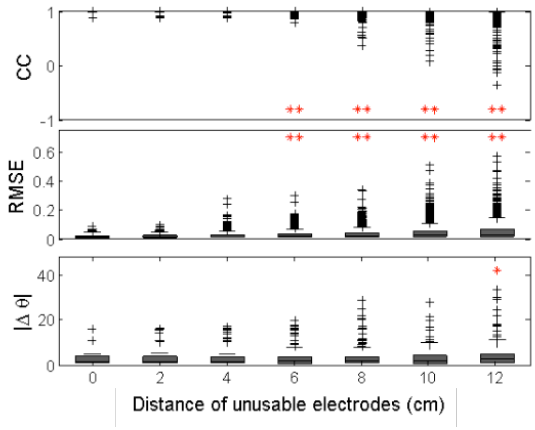

Fig 3. Comparison between true and reconstructed 12-lead ECG using simulated data with increasing number of unusable electrodes. Probability that distributions are significantly different to 0 cm: * $p<0.05$, ** $p<0.0001$.

3.2. Clinical Data

For patient data, the closest usable electrode to each ECG electrode was 1.6 [0-3.3] mm. The QRS and T-wave mean electrical axis were accurately captured for all patients (Table 1).

Reconstructed 12-lead ECGs demonstrated clinically relevant features allowing the correct diagnosis of all patients. For LBBB (Fig 4), this included broad and notched/slurred R-waves in leads I, aVL, V5 and V6, the absence of Q-waves in leads I and V5, and R-peak times >60 ms in leads V5 and V6.

Table 1. Comparison of $|\Delta\theta|$ for clinical data (n=6)

	QRS	T-wave
$\|\Delta\theta\|$	6.2 ± 4.7	14.2 ± 2.6

For NICD this included a prolonged QRS width (>120 ms), following a normally conduction p-wave, and morphology not pertaining to right or LBBB, or Wolf-Parkinson White syndrome. Fig 5 presents an example, with R-waves peaks at <60 ms and a deep S in V5 and V6, and the absence of R-waves in V1 and V2. While reconstructed ECGs produced an R-wave in V2, all other features were captured and NICD accurately diagnosed.

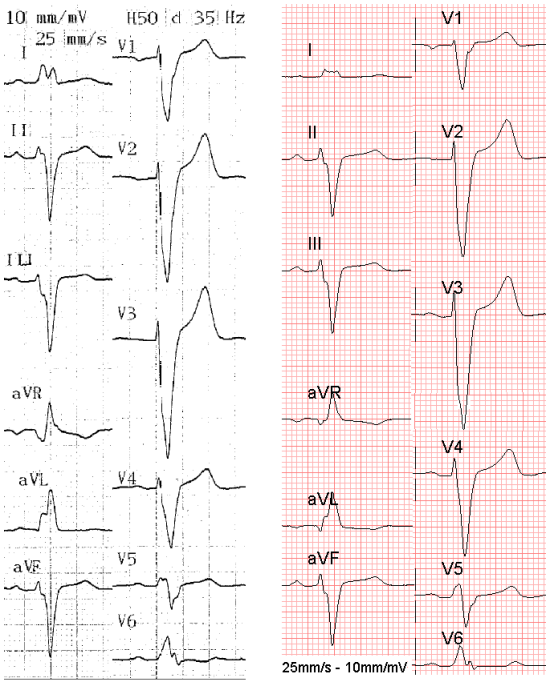

Fig 4. 12-lead ECG features indicating LBBB observed in the patient (left) captured by the reconstructed 12-lead ECG (right).

4. Discussion

The inverse-forward approach presented in this manuscript can accurately reconstruct 12-lead ECGs from BSPM, not only for overall morphology, amplitude, and mean electrical axis, but also for the small clinical features used in cardiac arrhythmia diagnosis.

The chest leads showed slightly more accurate reconstructions than the limb leads with simulated data (Figs. 2), though the difference in CC and RMSE values was not very substantial. This is likely because the chest leads lay in a more densely sampled region of the BSPM,

and thus are more likely to have all their source information captured.

On the other hand, with clinical data the reconstructed chest leads tended to show more differences than the limb leads when compared to the gold standard (Figs 4 and 5). As there was only a small number of unusable electrodes in each clinical case, these differences are likely due to the difference in reconstructed and gold-standard ECG lead locations (not present in simulated data).

Indeed, although the reconstructed ECG leads were placed according to recommended locations and CT-derived landmarks, previous studies have found there can be large inter-user variability particularly in the chest electrodes [12]. However, despite the small difference in these leads with the change in position, the important clinical features were always present in reconstructed 12-lead ECG allowing correct diagnosis.

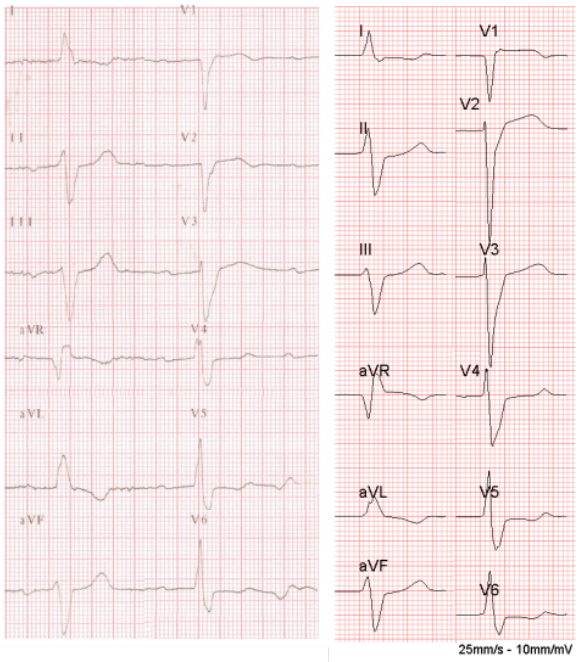

Fig 5. 12-lead ECG features indicating NICD observed in patient (left) captured by the reconstructed 12-lead ECG (right).

The ability of this approach to produce accurate 12-lead ECG reconstructions, even in the presence of relatively large regions of missing data (Fig 3), is likely not possible with other interpolation methods, which produce large inaccuracies in regions as small as 20 cm^2 [4]. The inverse-forward approach however, is based on fact the potential distribution on an internal surface can be seen as the source for the entire torso surface. The source generating the 12-lead ECG is also reflecting in electrodes in other regions of the body surface. It is then possible to estimate, by solving an inverse problem, the source elements that produce the missing electrodes, even when they are no present in the BSPM.

Whilst we have used this method here to reconstruct a 12-lead ECG, it is likely this method could also be used to derive other lead systems, such as the Frank lead system to obtain orthogonal leads.

Acknowledgements

This work was supported in part by La fondation Coeur et Artères under the grant number FCA14T2 and the French National Research Agency under Contract ANR-10-IAHU04-LIRYC.

References

[1] Rodrigo M, Guillem MS, Climent AL, Pedrón-Torrecilla J, Liberos A, Millet J, Fernández-Avilés F, Atienza F, Berenfeld O. Body surface localization of left and right atrial high-frequency rotors in atrial fibrillation patients: A clinical-computational study. *Heart Rhythm*, 2014:11(9);1584–91.

[2] Bear LR, Cuculich PS, Bernus O, Efimov I, Dubois R. Introduction to Noninvasive Cardiac Mapping. *Cardiac Electrophysiology Clinics*. 2015:7(1);1–16.

[3] Herman MV, Ingram DA, Levy JA, Cook JR, Athans RJ. Variability of electrocardiographic precordial lead placement: a method to improve accuracy and reliability. *Clinical cardiology*. 1991:14(6);469–476.

[4] J. E. Burnes, D. C. Kaelber, B. Taccardi, R. L. Lux, P. R. Ershler, and Y. Rudy, "A Field-Compatible Method for Interpolating Biopotentials," *Ann. Biomed. Eng*, vol. 26, no. 1, pp. 37–47, Jan. 1998.

[5] Wang Y, Rudy Y. Application of method of fundamental solutions to potential-based inverse electrocardiography. *Ann. Biomed. Eng*. 2006:34(8);1272–88.

[6] Tikhonov A, Arsenin V. *Solution of ill-posed problems*. Washington, D.C: John Wiley & Sons, 1977.

[7] Colli-Franzone PC, et al., Finite element approximation of regularized solutions of the inverse potential problem of electrocardiography and applications to experimental data. *Calcolo*. 1985:22(1);91–186.

[8] Ten Tusscher KHWJ. A Model for Human Ventricular Tissue. *AJP Heart Circ Physiol*. 2003:286(4);H1573–89.

[9] Krause D, Potse M, Dickopf T, Krause R, Auricchio A, Prinzen FW. Hybrid Parallelization of a Large-Scale Heart Model. LNCS 2012;7174:120-132.

[10] Surawicz R, Childers BJ, Deal LS, Gettes JJ, Bailey A, Gorgels EW, Hancock M, Josephson P, Kligfield JA, Kors P, Macfarlane JW, Mason DM, Mirvis P, Okin O, AHA/ACCF/HRS recommendations for the standardization and interpretation of the electrocardiogram Part III. *JACC*. 2009:53(11);976–981.

[11] Singh PN, Sajjad MA. Simplified calculation of mean QRS vector (mean electrical axis of heart) of electrocardiogram. *Indian Journal of Physiology and Pharmacology*. 2003:47(2);212–216.

[12] Rajaganeshan R, Ludlam CL, Francis DP, Parasramka SV, Sutton R. Accuracy in ECG lead placement among technicians, nurses, general physicians and cardiologists. *International journal of clinical practice*. 2008:62(1);65–70.

Dr. Laura Bear.
IHU-Liryc, Hôpital Xavier Arnozan, 33600 Pessac, France.
laura.bear@ihu-liryc.fr